Concentric Tesselation Maps and Curvature Continuous Guided Surfaces

K. Karčiauskas and J. Peters

October 23, 2006

Abstract

A multi-sided hole in a surface can be filled by a sequence of nested, smoothly joined surface rings. We show how to generate such a sequence so that (i) the resulting surface is C^2 (also in the limit), (ii) the rings consist of standard splines of moderate degree and (iii) the hole filling closely follows the shape of and replaces a guide surface whose good shape is desirable, but whose representation is undesirable.

To preserve the shape, the guided rings sample position and higher-order derivatives of the guide surface at parameters defined and weighted by a concentric tesselating map. A *concentric tesselating map* maps the domains of n patches to an annulus in $\mathbb{R}^2$ that joins smoothly with a λ-scaled copy of itself, $0 < \lambda < 1$. The union of λ^m-scaled copies parametrizes a neighborhood of the origin and the map thereby relates the domains of the surface rings to that of the guide.

The approach applies to and is implemented for a variety of splines and layouts including the three-direction box spline (with Δ-sprocket, e.g. Loop layout, at extraordinary points), tensor-product splines ($\square$-sprocket layout, e.g. Catmull-Clark), and polar layout. For different patch types and layout, the approach results in curvature continuous surfaces of degree less or equal 8, less or equal to (6,6), and as low as (4,3) if we allow geometric continuity.

1 Introduction and Motivation

A *guided surface ring* is a low-degree, piecewise polynomial or rational spline approximation to a ring-shaped region of an existing surface piece, called *guide*

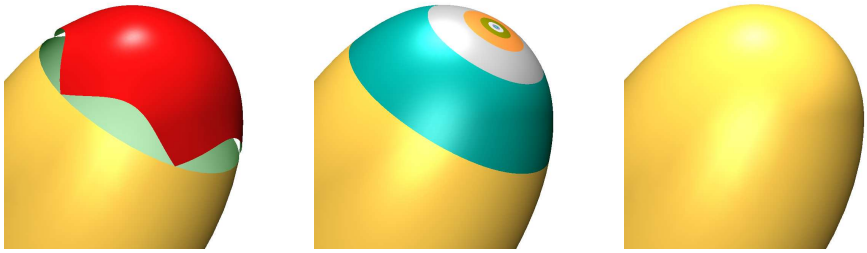

Figure 1: (*left*) Guide surface approximately capping a cylindrical body; (*middle*) color-coded sequence of guided rings and (*right*) uniformly shaded surface.

in the following. The guided rings are constructed to replace a guide that does not fit functional requirements or the requirements of a geometry processing pipeline. For example as illustrated in Figure 1, *left*, the guide may not exactly match the boundary data but overlaps or leaves gaps; or, the guide is of too high a degree or has an otherwise undesirable representation. The guide is replaced by a sequence of nested, smoothly joined surface rings in standard, say low-degree polynomial representation as in Figure 2.

The specific approach, detailed in this paper, is to generate guided rings $\mathbf{x}^m$ by applying an operator H that samples position and higher-order derivatives of a guide surface $\mathbf{g}$ at parameters defined and weighted by λ^m-scaled copies of a concentric tesselation map (short: *ct-map*) ρ:

$$\mathbf{x}^m := H(\mathbf{g} \circ \lambda^m \rho).$$

The ct-map maps the domains of n patches to an annulus in $\mathbb{R}^2$ so that the annulus and its λ-scaled copy, for some fixed $0 < \lambda < 1$, join smoothly and without overlap; and their union covers and parameterizes a disk around the origin (Figure 4, *top*). This disk relates the domain of the surface rings to that of

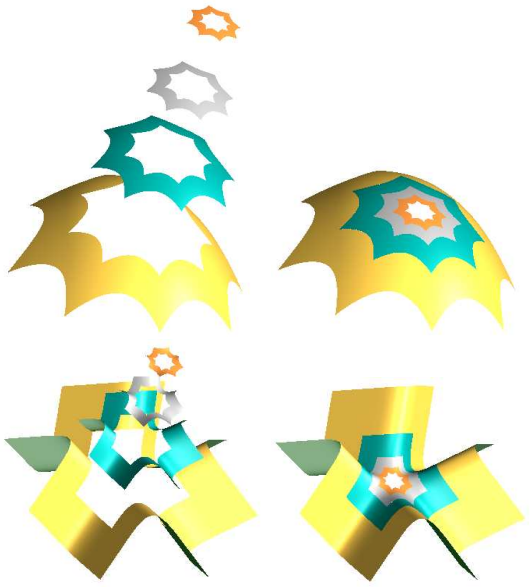

Figure 2: (*left*) Two sequences of guided rings, and (*right*) the resulting surfaces.

the guide. The ct-map is crucial to orient and scale higher-order derivatives taken off the guide surface. The operator H samples the guide surface and assures that consecutive rings $\mathbf{x}^m, \mathbf{x}^{m+1}$ join smoothly (Figure 2). The outermost ring, $\mathbf{x}^0$, smoothly joins the multi-sided boundary data.

The ringed structure of the surface yields a recurrence similar to standard subdivision. In Section 6, we show that the finite union of guided rings is a C^2 surface that reproduces quadratic components of the guide and that the infinite union is also C^2. An analysis of related useful, curvature bounded schemes and non-stationary C^2 schemes of lower degree will appear in [KP06a].

The choice of guide surface is important and, by definition, determines the shape of the guided rings. Only if the guide surface is properly fitted to the boundary data do the guided rings blend the existing multi-sided boundary data with the central guide without introducing new shape. Figure 3 illustrates how low-degree polynomials fail as a guides for higher-order saddles. Over the last four years,

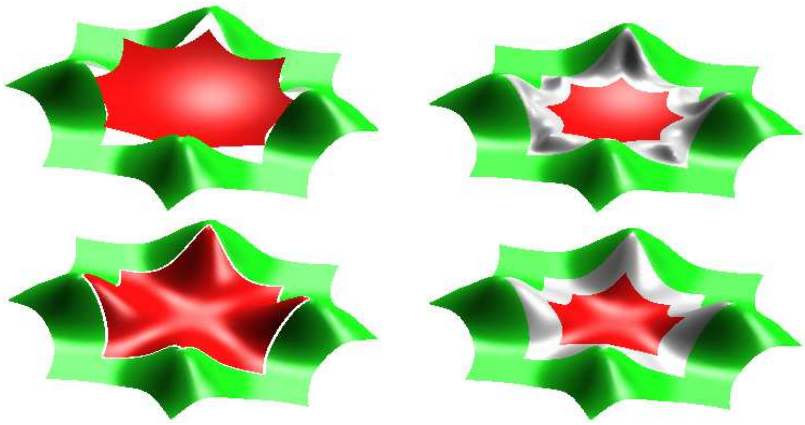

Figure 3: Choosing a good guide surface. Two different guides (8-sided inner pieces, *red*) are obtained by least-squares fitting to the same tensor-product spline data (outer ring, *green*). The guides are trimmed along the boundary of the ct-map ρ_C (see Section 5.2). (*top row*) Guide of degree three. (*bottom row*) Guide of *piecewise* degree five. (*right column*) Guided C^2 surfaces based on the guides on the left. Note the extra oscillations in the middle (*grey*) ring of the *top* surface based on the guide of degree three.

we developed and compared a number of high-quality guides, both high-degree rational [KP04] and piecewise polynomial. Since many other guide surfaces are possible, and a recommendation should be based on a thorough definition and

discussion of 'surface fairness' and a comprehensive comparison on standard test cases, we do not discuss guide constructions in detail but only assume that the guide is non-singular, at least twice continuously differentiable (see however (iii) in Section 8) and that its derivatives can be sampled up to the required order.

To recap, the two main reasons to generate guided rings are:

• to obtain a smooth, low-degree standard (piecewise polynomial) representation;

• to capture the shape of a complex guide surface.

Section 3 defines several ct-maps ρ. Section 4 defines the operator h that is modified to H in Section 5 to assemble the pieces $\mathbf{x}_i^m$ into guided rings $\{\mathbf{x}^m\}$ of a C^2 guided patchwork. Section 6 summarizes the continuity and shape reproduction properties of the patchworks and their limit, and points out how the rings are efficiently computed. Section 7 shows how the polynomial degree of polar rings can be lowered and Section 8 points out a number of modifications and generalizations of the approach explained in this paper.

2 Background

The main ingredients of guided ring-construction are composition and sampling ((quasi-)interpolation). No list of references would do justice to such fundamental techniques. Here, we focus on papers that influenced and informed the particular approach. First there are constructions like [KP04] that provide good shape for multi-sided surface patches but are of high rational degree. Then there is the observation that standard, mesh-based subdivision constructions offer low degree but yield potentially bad shape [KPR04], especially when the intent is to model convex surfaces. Thirdly, the analysis of subdivision surface motivates guided ring-constructions by its characterization of subdivision surfaces as a sequence of nested spline rings converging to an extraordinary point (see e.g. [Rei95]). If the guide surface, $\mathbf{g} : \mathbb{R}^2 \to \mathbb{R}^3$ were a single, not a piecewise polynomial and H exactly reproduced the composition $\mathbf{g} \circ \lambda^m \rho$ then the guided ring-construction would reduce to the approach in [Pra97, Rei98]. However, in guided ring-construction, the composition of guide and the ct-map is not used directly but *sampled*. That makes a difference since it allows to capture shape well, for example with high-degree piecewise polynomial maps, and still arrive at a low-degree representation – by leveraging standard spline theory. Low-degree (piecewise) polynomial mappings are known to create surfaces with curvature flaws. For example, a quadratic polynomial does not allow for a higher-order saddle to be modeled. Single polynomial guides also cannot model piecewise constant data; fitting to such data

typically leads to oscillations. Sampling is also fundamentally different from blending. Blending typically creates features not present in either the guide or the surrounding patch complex.

3 C^2 concentric tesselation maps

Tesselation means covering without overlap. A concentric tesselation map (short: ct-map) maps n copies of a *sector domain* S to an annulus in the plane:

$$\rho : S \times \{1, \ldots, n\} \to \mathbb{R}^2,$$

so that scaled copies of this annulus join without overlap to fill a disk around the origin. Moreover, the annulus parametrizations join smoothly. We explain maps for three types of domain S. The structure of the first two will be familiar to a reader who has seen Catmull-Clark and Loop's subdivision. The third, polar structure, was introduced in [KP06b]. Let $\square$ be the unit square, Δ the unit triangle and

$$\mathsf{c} := \cos\alpha, \quad \alpha := 2\pi/n.$$

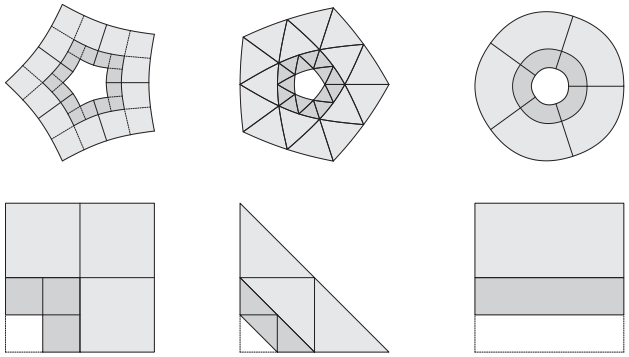

Figure 4: The *top* row shows tesselating annuli generated by ct-maps ρ and $\lambda\rho$. The *bottom* row shows S and $S/2$ used for the prolongation $\rho(S/2) := \lambda\rho(S)$. (*left*) $\square$-sprocket (Catmull-Clark subdivision) layout; (*middle*) $\triangle$-sprocket (Loop subdivision) layout; (*right*) polar layout ($S/2$ is interpreted as halving only the vertical direction).

- The ct-map ρ_C is the characteristic map of Catmull-Clark subdivision (see e.g. [PR98]). It maps n copies of the domain $S := 2\square - \square \simeq \square \times \{1, 2, 3\}$

(Figure 4, *left bottom*) to an annulus (Figure 4, *left top*). The annulus is bounded by n spline curves joining with internal corners. If we fix scaling and rotation, ρ_C is uniquely determined. The scale factor λ is the subdominant eigenvalue of the Catmull-Clark subdivision:

$$\lambda = \lambda_C := (\mathsf{c} + 5 + \sqrt{(\mathsf{c}+9)(\mathsf{c}+1)})/16.$$

It is the unique factor so that $\rho_C(\frac{s}{2}, \frac{t}{2}) := \lambda\rho_C(s,t)$ is a C^2 prolongation of ρ_C. $(*)$ *Here and in the following, we say ρ and $\lambda\rho$ join C^2, although, formally, we have to subdivide ρ once to have matching derivatives.*

- The ct-map ρ_L, shown in Figure 4, *top middle*), is the characteristic map of Loop's subdivision (see e.g. [Uml99]). It maps n copies of $S := 2\Delta - \Delta \simeq \Delta \times \{1,2,3\}$ to an annulus bounded by n spline curves joining with internal corners. If we fix scaling and rotation, ρ_L is uniquely determined. The unique scale factor, that allows C^2 prolongation of ρ_L and thereby tesselating the neighborhood of the origin, is the subdominant eigenvalue of the Loop's subdivision,

$$\lambda = \lambda_L := (3 + 2\mathsf{c})/8.$$

- For the third, the polar layout, we define two alternative ct-maps. Both act on $S := ([0..2] \times [1..2]) \simeq \square$ and yield an annulus bounded by a single spline consisting of n smoothly joining pieces (Figure 4, *top right*). Both polar ct-maps are periodic strips of tensor-product splines that are linear in the radial direction. A strip is defined by two B-spline control polygons, each with n control points uniformly distributed on the scaled unit circle. The points of the first ct-map, ρ_p, are interpreted as (the two coordinates of) cubic B-spline coefficients, defining a C^2 map of degree (3,1). The points of the second ct-map, ρ_g, are interpreted as uniform quadratic B-spline coefficients, making the map of degree (2,1) and C^1 and, due to symmetry, G^2. Both can alternatively be defined in Bézier form.

  The Bézier control points of the ith segment of ρ_p are defined by rotating a template patch r by $i\alpha$ about the origin. The template patch is of degree 3 in 'circular' and degree 1 in the 'radial' direction and its coefficients $r_{kj} \in \mathbb{R}^2$, $k = 0,1,2,3$, $j = 0,1$ are defined with the help of the reflection R_α across the line through the origin and $[\cos\frac{\alpha}{2}, \sin\frac{\alpha}{2}]$ (cf. Figure 5, *left*):

$$r_{00} := \left[\begin{smallmatrix}1\\0\end{smallmatrix}\right], r_{10} := \left[\begin{smallmatrix}1\\ \frac{\sin\alpha}{2+\cos\alpha}\end{smallmatrix}\right],\ r_{20} := R_\alpha r_{10},\ r_{30} := R_\alpha r_{00} = \left[\begin{smallmatrix}\cos\alpha\\ \sin\alpha\end{smallmatrix}\right],$$
$$r_{k1} := \lambda r_{k0}.$$

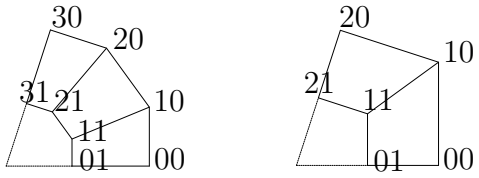

Figure 5: Bézier coefficients of one segment of two polar ct-maps. (*left*) The C^2 ct-map ρ_p of degree (3,1). (*right*) The G^2 ct-map ρ_g of degree (2,1).

By construction, the polynomial pieces of ρ_p join C^2.

Similarly, the ct-map ρ_g has a template r (see Figure 5, *right*)

$$r_{00} := \left[\begin{smallmatrix} 1 \\ 0 \end{smallmatrix}\right] , \quad r_{10} := \left[\begin{smallmatrix} 1 \\ \tan(\alpha/2) \end{smallmatrix}\right] , \quad r_{20} = \left[\begin{smallmatrix} \cos\alpha \\ \sin\alpha \end{smallmatrix}\right] , \qquad r_{i1} = \lambda r_{i0}.$$

For both $\rho = \rho_p$ and $\rho = \rho_g$, any choice of $0 < \lambda < 1$ will yield a C^2 prolongation. The simplest choice, $\lambda = 1/2$, is the default scaling factor.

In all cases, not only do the annuli, as sets in $\mathbb{R}^2$, tesselate the neighborhood of the origin, but ρ and $\lambda\rho$ join smoothly. Internally, each ring is C^2 except for the pieces ρ_g^i that join with curvature continuity as follows.

Lemma 1 *The segments $\rho_g^i, i = 0, \ldots, n-1$ of ρ_g are C^1 and G^2 connected:*

$$\partial_s^2 \rho_g^{i+1}(0,t) = \partial_s^2 \rho_g^i(1,t) + k_2 \partial_s \rho_g^i(1,t), \qquad k_2 := 2\cos\alpha - 2.$$

We summarize the ct-maps and their properties in Table 1.

Table 1: Three C^2 and one G^2 ct-map.

symbol	**degree**	λ **scale**	**layout**
ρ_C	(3,3)	λ_C	Catmull-Clark
ρ_L	4	λ_L	Loop
ρ_p	(3,1)	1/2	polar
ρ_g	(2,1)	1/2	polar

4 Sampling operators

The sampling operator h (not yet H) for tensor-product patches determines a tensor-product patch $h(f)$ in Bézier form, matching the derivatives of a given map f defined on $\square$ at the four corners, at least up to second order.

- The simplest operator, h^{55} generates a patch of degree $(5,5)$. For each corner, it samples the partial derivatives, the (2,2)-jet of f,

$$\begin{matrix} f & \partial_s f & \partial_s^2 f \\ \partial_t f & \partial_s \partial_t f & \partial_s^2 \partial_t f \\ \partial_t^2 f & \partial_s \partial_t^2 f & \partial_s^2 \partial_t^2 f \end{matrix},$$

  rerepresents them by its 3×3 expansion in Bézier form. Together these four groups of nine coefficients define the 36 coefficients of patch of degree $(5,5)$ (Figure 6, *left*).

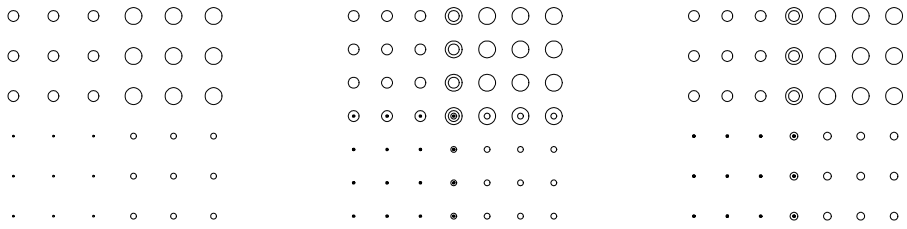

Figure 6: (*left*) Combining four (2,2)-jets in Bézier form into a segment $\mathbf{x}_j^m$ of a polynomial patch of degree (5,5). (*middle*) Averaging (3,3)-jets to define a patch of degree (6,6). (*right*) Averaging (3,2)-jets to define a patch of degree (6,5).

Off hand, the guide must be at least $C^{2,2}$ at the sample points for the tensor 2-jet to be well-defined (see, however, generalization (iii) at the end of this paper). For the specific construction, we guarantee well-definedness of the tensor jet and higher-order jets by making the rays that form the segment boundaries of the ct-map (see Figure 7) match the domain boundaries of the polynomial pieces of the guide. While the operator h^{55} approximates the geometry of the guide surface well and suffices to create a sequence of C^2 joined C^2 rings, we generally need operators of slightly higher degree to create C^2 surfaces in the limit. In particular, for Lemma 4, the operator has to reproduce certain polynomials $\mathbf{q} \circ \rho$ of degree $(6,6)$ or total degree 8.

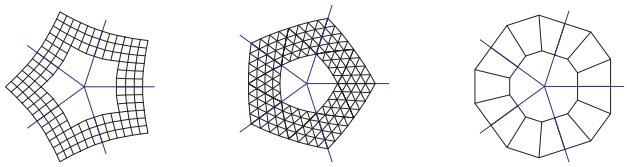

Figure 7: Three types of ct-maps: ρ_C, ρ_L, ρ_p. In each case, the rays emanating from the center are aligned with the sector boundaries of the domain of the piecewise polynomial map $\mathbf{g}$.

- The operator h^{66} samples partial derivatives up to third order, converts into 4×4 corner blocks of Bézier coefficients of degree $(6, 6)$ and averages coefficients at overlapping positions, to form a patch of degree $(6, 6)$ (Figure 6, *middle*).

- The operator h^{65} samples up to third order in one and up to second order in the other direction and then averages overlapping entries of the 4×3 corner blocks to form a patch of degree $(6, 5)$ (cf. Figure 6, *right*).

The operator h^8 (not yet H) for polynomial pieces of total degree (triangular patches) is as follows.

- The sampling operator h^8, for patches of total degree eight, collects the partial derivatives

$$(\partial_s^i \partial_t^j f)_{0 \le i+j \le 4}, \partial_s^3 \partial_t^2 f, \partial_s^3 \partial_t^2 f,$$

  and converts them into 17 Bézier coefficients filling a corner of the coefficient array of a polynomial of degree 8 in Bézier form. As illustrated in

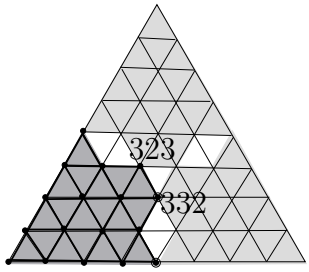

Figure 8: The operator h^8 determines the Bézier points of the bold submesh. Three such submeshes define a polynomial piece of degree 8. Points in positions of overlap, 323, 332, 233, are averaged.

Figure 8, overlapping coefficients are averaged, and three operators define a patch of degree 8.

5 Guided patchworks

We now define a guided ring, $\mathbf{x}^m = H(f)$ where $f = \mathbf{g} \circ \lambda^m \rho$, ρ is a ct-map and

$$\mathbf{g} : \mathbb{R}^2 \to \mathbb{R}^3, \quad (u, v) \mapsto (x, y, z).$$

The contraction of the smoothly connected rings $\{\lambda^m \rho\}_m$ is inherited by the sequence of compositions $\{\mathbf{g} \circ \lambda^m \rho\}_m$ and the sampled C^2 guided rings $\mathbf{x}^m$ will join to form a C^2 (G^2) surface in $\mathbb{R}^3$ (cf. Remark ($*$) Section 3). There are a number of possible combinations of h and ρ and we focus on presenting the cases that have higher degree and consist of few polynomial pieces. Section 7 shows alternatives of lower-degree and more pieces.

5.1 Guided polar patchworks

We discuss two polar constructions. If $\rho = \rho_p$ then $H = h^{6,5}$; if $\rho = \rho_g$ then $H = h^{5,5}$.

Lemma 2 *If $\rho = \rho_p$ then the segments $\mathbf{x}_i^m$ and $\mathbf{x}_{i+1}^m$ join C^2. If $\rho = \rho_g$ then the segments $\mathbf{x}_i^m$ and $\mathbf{x}_{i+1}^m$ join C^1 and G^2. In both cases, $\mathbf{x}^m$ and $\mathbf{x}^{m+1}$ join C^2.*

Proof If $\rho = \rho_p$ then $\mathbf{g} \circ \lambda^m \rho$ is C^2 and adjacent segments, $\mathbf{x}_i^m$ and $\mathbf{x}_{i+1}^m$, and $\mathbf{x}_i^m$ and $\mathbf{x}_i^{m+1}$ share the same second-order expansion where they join. If $\rho = \rho_g$ then, by Lemma 1, ρ is C^1 and hence

$$\partial_s(\mathbf{g} \circ \rho_{i+1}^m)(0, t) = \partial_s(\mathbf{g} \circ \rho_i^m)(1, t) \ .$$

Since k_2 is a constant,

$$\partial_s^2(\mathbf{g} \circ \lambda^m \rho^{i+1})(0, t) = \partial_s^2(\mathbf{g} \circ \lambda^m \rho^i)(1, t) + k_2 \partial_s(\mathbf{g} \circ \lambda^m \rho^i)(1, t) \ .$$

That is, circularly adjacent segments of $\mathbf{g} \circ \lambda^m \rho$ are C^1 and G^2 connected. It remains to show that this property is preserved by H. Neighboring patches $\mathbf{x}_i^m$ and $\mathbf{x}_{i+1}^m$ match the expansion of $\mathbf{g} \circ \lambda^m \rho$ at the two endpoints, and the transversal expansions have the same structure. Since k_2 does not vary with t,

$$\partial_s \mathbf{x}_{i+1}^m(0, t) = \partial_s \mathbf{x}_i^m(1, t) \ ,$$
$$\partial_s^2 \mathbf{x}_{i+1}^m(0, t) = \partial_s^2 \mathbf{x}_i^m(1, t) + k_2 \partial_s \mathbf{x}_i^m(1, t).$$

The final claim follows since $\lambda^m \rho$ and $\lambda^{m+1} \rho$ join C^2. |||

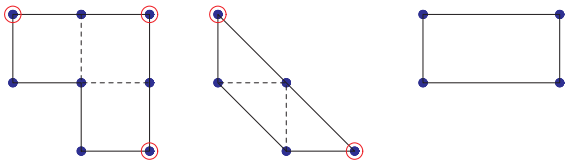

Figure 9: Sampling locations of $h(\mathbf{g} \circ \rho)$ for $\rho = \rho_C$ (*left*), ρ_L (*middle*) and ρ_p, ρ_g (*right*).

5.2 Guided Catmull-Clark patchworks

For $\rho = \rho_C$ and $h = h^{6,6}$, H samples $\mathbf{g} \circ \lambda^m \rho$ at the corners of the three elementary patches that make up each L-shaped segment (Figure 9, *left*). Arguments as in Lemma 2 show that adjacent L-shapes join to form a C^2 ring. But, although the actual difference is very small, adjacent rings are not smoothly connected. Therefore H replaces the three outermost layers of Bézier coefficients by a C^2 extension of the patch $\mathbf{x}_i^{m-1}$ (once subdivided to match the granularity). For $m = 0$, boundary data are extended. Figure 10 illustrates the algorithmic steps.

5.3 Guided Loop patchworks

We explain the combination of ρ_L and h^8 to create the operator H that generates, per sector, three C^2-joined triangular patches of total degree 8. The construction is similar to the previous construction in that we need to establish C^2 continuity across interior boundaries, segment boundaries and ring boundaries. We recall that, if two polynomial pieces $\mathbf{p}$ and $\tilde{\mathbf{p}}$ in triangular Bézier form join along an

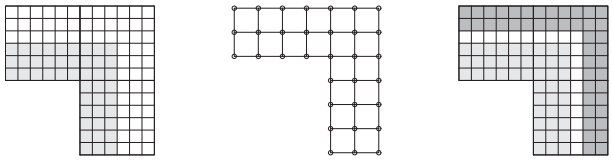

Figure 10: Construction of Catmull-Clark guided ring: (*left*) $h^{6,6}$ defines four layers of control points along the inward corner edges of patches of degree (6,6). (*middle*) The three outermost layers of a degree (6,6) patch, obtained by sampling a bicubic extension of the previous layer (at the circled points in Figure 9, *left*) are subdivided to match the granularity of the points generated by $h^{6,6}$ (*right*).

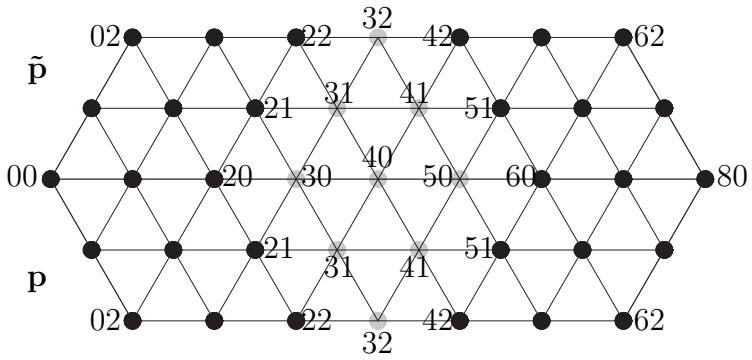

Figure 11: Indexing of three layers of Bézier coefficients $i0$, $j1$ and $k2$ of two (triangular) patches $\mathbf{p}$ and $\tilde{\mathbf{p}}$ of degree 8 that join along a common boundary $00--80$ with indices $i0$, $i = 0, \ldots, 8$.

edge $\mathbf{p}_{j0} = \tilde{\mathbf{p}}_{j0}$, $j = 0, \ldots, 8$, then the C^1 and C^2 constraints respectively are

$$\tilde{\mathbf{p}}_{j1} = -\mathbf{p}_{j1} + \mathbf{p}_{j0} + \mathbf{p}_{j+1,0}, \quad j = 0, \ldots, 7 \tag{1}$$

$$\begin{aligned} \tilde{\mathbf{p}}_{j2} &= \mathbf{p}_{j2} - 2\mathbf{p}_{j1} - 2\mathbf{p}_{j+1,1} + \mathbf{p}_{j0} + 2\mathbf{p}_{j+1,0} + \mathbf{p}_{j+2,0}, \\ &= \tilde{\mathbf{p}}_{j1} - \mathbf{p}_{j1} + \tilde{\mathbf{p}}_{j+1,1} - \mathbf{p}_{j+1,1}, \qquad j = 0, \ldots, 6. \end{aligned} \tag{2}$$

These rules can directly be applied to prolong the existing patch complex $\mathbf{p}$ to a piece $\tilde{\mathbf{p}}$ of the ring (Figures 11 and 12, *top right*). Across all other ring boundaries, segment boundaries and interior boundaries, imposing the C^2 constraints results in an underconstrained problem since both $\mathbf{p}$ and $\tilde{\mathbf{p}}$ can be adjusted. The following symmetric modification $\mathbf{p}_{ij}^{\text{new}}$ and $\tilde{\mathbf{p}}_{ij}^{\text{new}}$ of coefficients $\mathbf{p}_{ij}$ and $\tilde{\mathbf{p}}_{ij}$ initialized by h^8 leaves $\mathbf{p}_{40}$ unchanged:

$$\begin{aligned} \xi &:= \frac{\mathbf{p}_{40} - \mathbf{p}_{20}}{2}, \dot{\xi} := \frac{\mathbf{p}_{21} - \tilde{\mathbf{p}}_{21}}{2}, \ddot{\xi} := \frac{\mathbf{p}_{22} - \tilde{\mathbf{p}}_{22}}{2}, \qquad \bar{p} := \frac{\mathbf{p}_{32} + \tilde{\mathbf{p}}_{32}}{2}, \\ \eta &:= \frac{\mathbf{p}_{40} - \mathbf{p}_{60}}{2}, \dot{\eta} := \frac{\mathbf{p}_{51} - \tilde{\mathbf{p}}_{51}}{2}, \ddot{\eta} := \frac{\mathbf{p}_{42} - \tilde{\mathbf{p}}_{42}}{2}. \end{aligned}$$

$$\begin{aligned} \mathbf{p}_{31}^{\text{new}} &:= \tilde{\mathbf{p}}_{21} + \xi + \ddot{\xi}, \ \mathbf{p}_{41}^{\text{new}} := \tilde{\mathbf{p}}_{51} + \eta + \ddot{\eta}, \quad \mathbf{p}_{32}^{\text{new}} := \bar{p} - (\dot{\xi} + \dot{\eta}) + \ddot{\xi} + \ddot{\eta}; \\ \tilde{\mathbf{p}}_{31}^{\text{new}} &:= \mathbf{p}_{21} + \xi - \ddot{\xi}, \ \tilde{\mathbf{p}}_{41}^{\text{new}} := \mathbf{p}_{51} + \eta - \ddot{\eta}, \quad \tilde{\mathbf{p}}_{32}^{\text{new}} := \bar{p} + \dot{\xi} + \dot{\eta} - (\ddot{\xi} + \ddot{\eta}) \end{aligned} \tag{3}$$

(see Figure 11).

Application of the operator H consists of four steps illustrated in Figure 12. We label as A_i^m, B_i^m and C_i^m the polynomial pieces of degree 8 that make up a sector $\mathbf{x}_i^m$.

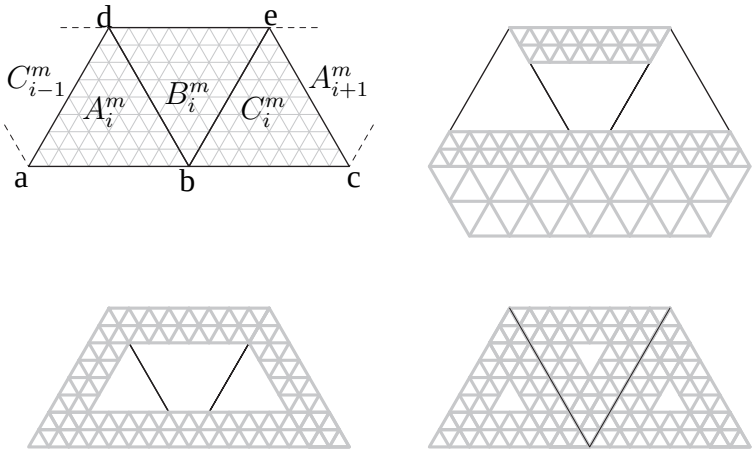

Figure 12: Steps 1 – 4 of the operator H generating three degree 8 patches per sector.

1. (Figure 12, *top left*): Apply the operator h^8 at a,b,…,e.

2. (Figure 12, *top right*): Across the ring boundary $\overline{B_i^{m-1}\,(A_i^m, C_i^m)}$,
   if $m = 0$ use the C^2 rules (1) and (2) to extrapolate the existing patch complex B_i^{-1} and obtain layers 0, 1 and 2 of Bézier coefficients of $\tilde{\mathbf{p}}$ across the ring boundary ($\tilde{\mathbf{p}}$ is not yet split into layers of A_i^m, B_i^m, C_i^m);
   if $m > 0$, apply the symmetric assignment of Equation (3) to obtain the three layers of coefficients of B_i^{m-1} and the adjacent layers of $\tilde{\mathbf{p}}$.
   Note that the innermost (topmost) layers of B_i^m are generated in the subsequent iteration.

   The layers of $\tilde{\mathbf{p}}$ are split (by subdivision) to define layers 0, 1, 2 of A_i^m and B_i^m and C_i^m. In general, this changes the h^8 data at b (at a and c, the coefficients remain identical to those of the local application of h^8). We adjust the points labeled B_{512} and B_{521} in Figure 13 to restore C^2 continuity along the interior edges emanating from b

$$B_{512}^{\text{new}} := \frac{B_{512} + B_{521}}{2} + \mathbf{k}, \qquad B_{521}^{\text{new}} := \frac{B_{512} + B_{521}}{2} - \mathbf{k},$$

$$\begin{aligned}\mathbf{k} :=& \frac{1}{512}\big(\tilde{\mathbf{p}}_{10} - \tilde{\mathbf{p}}_{70} + 4(\tilde{\mathbf{p}}_{20} - \tilde{\mathbf{p}}_{60}) + 5(\tilde{\mathbf{p}}_{30} - \tilde{\mathbf{p}}_{50}) \\ &+ \tilde{\mathbf{p}}_{01} - \tilde{\mathbf{p}}_{71} + 5(\tilde{\mathbf{p}}_{11} - \tilde{\mathbf{p}}_{61}) + 9(\tilde{\mathbf{p}}_{21} - \tilde{\mathbf{p}}_{51}) + 5(\tilde{\mathbf{p}}_{31} - \tilde{\mathbf{p}}_{41}) \\ &+ \tilde{\mathbf{p}}_{02} - \tilde{\mathbf{p}}_{62} + 4(\tilde{\mathbf{p}}_{12} - \tilde{\mathbf{p}}_{52}) + 5(\tilde{\mathbf{p}}_{22} - \tilde{\mathbf{p}}_{42})\big)\,,\end{aligned}$$

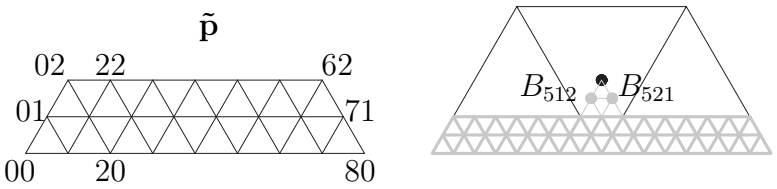

Figure 13: Additional illustration of Step 2. (*left*) Extrapolated layers of $\tilde{\mathbf{p}}$ (cf. Figure 11). (*right*) Modification of coefficients to satisfy the requirements of Lemma 4 (cf. Figure 12, *top right*).

and then recompute their neighbors B^{new}_{503} and B^{new}_{530} on the edges to enforce the C^1 constraints.

3. (Figure 12, *bottom left*): Across the segment boundary $\overline{C^m_{i-1}\ A^m_i}$, apply the symmetric assignment of Equation (3).

4. (Figure 12, *bottom right*): Across the interior boundary $\overline{A^m_i\ B^m_i}$ and across $\overline{B^m_i\ C^m_i}$ apply the symmetric assignment of Equation (3).

Steps 3 and 4 ensure that each ring $\mathbf{x}^m$ is C^2 and Step 2 insures that the rings $\mathbf{x}^m$ and $\mathbf{x}^{m+1}$ are C^2-connected and $\mathbf{x}^0$ is C^2-connected to the surrounding spline surface.

6 Properties of Patchworks

A patchwork is the finite union $\bigcup_{m<m_0, i\in\mathbb{Z}_n} \mathbf{x}^m_i$ of segments $\mathbf{x}^m_i$ as defined in the previous section by (ρ, h) and their correction by H. We summarize the results of Section 5.

Lemma 3 (Second order continuity of patchworks) *The patchworks defined by any of $(\rho_C, h^{6,6})$, (ρ_L, h^8) or $(\rho_p, h^{6,5})$ and H are C^2. The patchwork defined by $(\rho_g, h^{5,5})$ is curvature continuous.*

To see how well the guided rings capture shape, we show that guided rings reproduce compositions with quadratic guide surfaces. Denote by $\mathbf{g}_{i;k}$ the homogeneous part of degree k of $\mathbf{g}_i$. That is $\mathbf{g}_{i;k}$ is a linear combination of monomials of total degree k in the expansion of the ith segment of $\mathbf{g}$ with respect to the parameters (u, v). Then $\mathbf{g}_{i;k}(\lambda\cdot) = \lambda^k \mathbf{g}_{i;k}$ and,

$$\text{for } m > 0, \quad \mathbf{x}^m_{i;k} = H(\mathbf{g}_{i;k} \circ \lambda^m \rho) = \lambda^{mk} H(\mathbf{g}_{i;k} \circ \rho). \tag{4}$$

This yields the decomposition ($\mathbf{x}^0$ is perturbed by the boundary data)

$$\mathbf{x}_i^m = \sum_{k=0}^{d} \lambda^{(m-1)k} \mathbf{x}_{i;k}^1 \ . \tag{5}$$

Lemma 4 (Reproduction) *For $m > 0$,*

$$\mathbf{x}_{i;0}^m + \mathbf{x}_{i;1}^m + \mathbf{x}_{i;2}^m = (\mathbf{g}_{i,0} + \mathbf{g}_{i,1} + \mathbf{g}_{i,2}) \circ \lambda^m \rho \ . \tag{6}$$

Proof The patchwork is completely defined by the composition $\mathbf{g} \circ \lambda\rho$. If the degree of $\mathbf{x}_{i;k}^m$ exceeds the degree of $\mathbf{g}_{i,k} \circ \lambda^m \rho$, the latter is reproduced by sampling. By definition, degree $\mathbf{g}_{i,k} = k$, and the degree of ρ is one of $(3,3)$, $(3,1)$, $(2,1)$ and 4, so that degree$((\mathbf{g}_{i,0} + \mathbf{g}_{i,1} + \mathbf{g}_{i,2}) \circ \lambda^m \rho) = 2$ degree$(\rho) \leq$ degree$(\mathbf{x}_{i;0}^m + \mathbf{x}_{i;1}^m + \mathbf{x}_{i;2}^m)$. |||

By construction, the operators H generate rings $\mathbf{x}^m$ of sufficient degree to reproduce $\mathbf{q}\lambda^m\rho$ where $\mathbf{q}$ is any polynomial of degree 2. By assumption, the guide $\mathbf{g}$ is twice continuously differentiable at $(0,0)$ and sufficiently smooth at the sampling sites. Together, this implies curvature continuity of the infinite union of guided rings.

Theorem 1 (Curvature continuous Guided Subdivision) *The infinite union of guided rings, $\bigcup_{m\in\mathbb{N},i\in\mathbb{Z}_n} \mathbf{x}_i^m$, of the four types listed in Lemma 3 form a C^2 surface. The second-order expansion at the limit point $\mathbf{x}_i^\infty$ matches that of $\mathbf{g}$.*

Proof We define a new parametrization $\mathbf{y}(u,v)$ of $\mathbf{x} = \cup\mathbf{x}^m$ as

$$\mathbf{y}_i^m(u,v) := \mathbf{x}_i^m(s,t), \quad (u,v) := \lambda^m \rho_i(s,t),$$

where i enumerates the sectors. Then $\mathbf{y}$ is defined on a punctured disk surrounding but excluding the origin. From decomposition (5)

$$\mathbf{y}_i(u,v) = \sum_{k=0}^{d} \mathbf{y}_{i;k}(u,v) \ , \tag{7}$$

where the functions $\mathbf{y}_{i;k}$ satisfy

$$\mathbf{y}_{i;k}(\lambda u, \lambda v) = \lambda^k \mathbf{y}_{i;k}(u,v) \ . \tag{8}$$

Due to C^2 continuity of the guide, the second order expansions of each sector, $\mathbf{g}_{i,0} + \mathbf{g}_{i,1} + \mathbf{g}_{i,2}$, are part of a single quadratic polynomial

$$\mathbf{q}(u,v) = \mathbf{a}_0 + \mathbf{a}_1 u + \mathbf{a}_2 v + \mathbf{a}_3 u^2 + \mathbf{a}_4 uv + \mathbf{a}_5 v^2,$$

and, by Lemma 4, the decomposition (7) has the form

$$\mathbf{y}_i(u,v) = \mathbf{q}_i(u,v) + \sum_{k=3}^{d} \mathbf{y}_{i;k}(u,v)\ . \tag{9}$$

where $\mathbf{q}_i$ is the restriction of $\mathbf{q}$ to the domain of $\mathbf{y}_i$. Differentiating (8), we get

$$\partial_u^\alpha \partial_v^\beta \mathbf{y}_{i;k}(\lambda u, \lambda v) = \lambda^{k-\alpha-\beta} \partial_u^\alpha \partial_v^\beta \mathbf{y}_{i;k}(u,v)\ , \quad \alpha+\beta < 3\ ,\ k \geq 3\ . \tag{10}$$

Then (9) and (8) imply that the rings $\mathbf{x}^m$ contract to a central point $\mathbf{g}(0,0) = \mathbf{a}_0$ of the guide surface. Setting $\mathbf{y}(0,0) := \mathbf{a}_0$, makes the parametrization $\mathbf{y}(u,v)$ continuous at the origin. By (9) and (10) the derivatives of $\mathbf{y}(u,v)$ up to order 2 have well-defined limits at $(0,0)$ and these coincide with the quadratic expansion $\mathbf{q}(u,v)$ of $\mathbf{g}$. |||

The parametrization $\mathbf{y}$ was pointed out in [Pra98] and the final argument is adapted from [WW02]. The parametrization $\mathbf{y}$ shows in particular that surfaces based on ρ_g are C^2 at the extraordinary point from the point of view of differential geometry.

Guided surfaces with $\square$-sprocket layout match the lower bound on the degree of curvature continuous subdivision surfaces [Rei96]. Curvature continuous guided polar subdivision surfaces of degree $(5,5)$ do not contradict this bound since the patch layout is different from the one assumed in [Rei96]. Section 7 shows that the polar layout allows reducing the radial degree to 3 and, replacing C^2 continuity by geometric G^2 continuity, degree 4 suffices in the circular direction. This yields curvature continuous guided surfaces of degree (4,3).

6.1 Efficient computation of polynomially guided rings

Consecutive guided rings can be computed efficiently and numerically stably by precalculated formulas if the guide is piecewise polynomial.

Observation 1 (Stationary rules) *If the guide is (piecewise) polynomial then the construction of the contracting guided patchwork rings is stationary.*

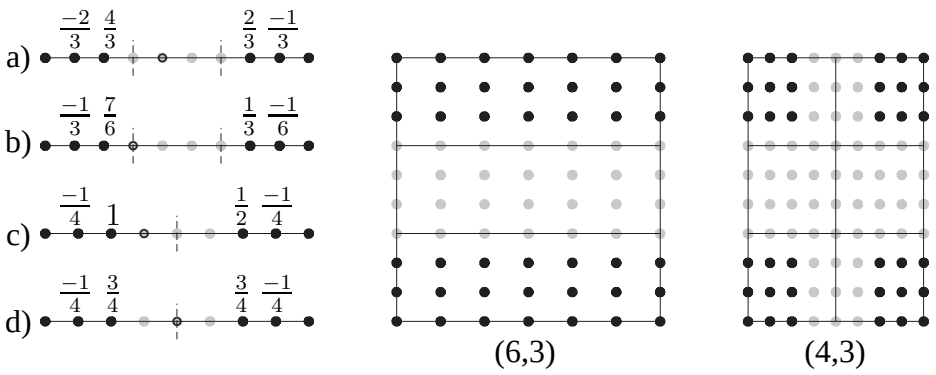

Figure 14: Hermite data merged to define macropatches of degree (i,j) and smoothness $C^{i-1,j-1}$. Formulas a) through d) define the unknown Bézier coefficients (*hollow circles*) in terms of given coefficients (*solid black disks*). Formulas a) and b) define Bézier coefficients of a C^2 cubic spline. Formulas c) and d) define Bézier coefficients of a C^3 spline of degree 4.

Proof Computing the restriction

$$\mathbf{g}_i(\lambda\cdot) := \Delta \to \mathbb{R}^3$$

of $\mathbf{g}_i$ to $\lambda\Delta$ involves only convex combinations since the Bézier points of a piece of the patch are convex combinations of the Bézier coefficients of the complete patch. This computation is numerically stable and the rules for determining $\mathbf{g}(\lambda^{m+1}\cdot)$ from $\mathbf{g}(\lambda^m\cdot)$ are the same as for determining $\mathbf{g}(\lambda\cdot)$ from $\mathbf{g}$. Given $\mathbf{f} := \mathbf{g}(\lambda^m\cdot)$, the rules for determining $H(\mathbf{f}\circ\rho)$ do not change with m. |||
We also note that Guided Subdivision has a fast evaluation algorithm based on the subdivision (4) and superposition (5) of eigenfunctions.

7 Spline-reduced low-degree sampling operators

Careful analysis shows that the degree of the patches in C^2 polar construction can be reduced to (6,4) and that of the G^2 construction to (4,4). However, we can reduce the degree of the sampled patches even further by choosing it as a spline rather than as a single polynomial and Lemma 3, Lemma 4, Observation 1 and hence Theorem 1 continue to hold. Figure 14 shows several options for polar operators that can be used with ρ_p and ρ_g, respectively. For example, position, first and second derivative at the ends, define a unique C^2 spline consisting of three cubic segments (Formulas for Bézier coefficients are given in a) and b)).

- Applying this procedure to h^{65} yields, for example, $h^{63}(f)$ consisting of three C^2 connected patches of degree (6,3) as shown in Figure 14 (6,3).

Instead of splitting the patch into three, a more complex analysis shows that two pieces suffice. Alternatively, we can construct a C^3 spline consisting of two degree 4 pieces by the formulas c) and d).

- Applying this procedure in one and the previous procedure in the other direction to h^{55} yields a Hermite interpolant h^{43} consisting of six C^2 connected patches of degree $(4,3)$ as shown in Figure 14 (4,3).

These lower-degree operators generate very similar surfaces to those in Section 4.

8 Generalizations

The practicality and good shape of the specific constructions of this paper have been verified by implementation (see e.g. Figure 15). Over a wide range of input data, guided rings consistently introduced fewer shape and curvature artifacts than an equal number of conventional, mesh-based subdivision steps. The implemented constructions presented in this paper are, however, only a small sample of many options, and, the reader may already have thought about extensions, modifications and generalizations for specific applications. Here we list a few that we have explored or considered over the last years.
(a) Higher smoothness requires higher-order ct-maps and higher-order sampling.
(b) Some other form of (quasi-)interpolation can replace the jet-sampling of the operator H. In particular,
(c) the proof of Theorem 1 points to the fact that guides need not be C^2 except for a common quadratic jet (common expansion) at the central point (cf. [KMP06]). The operator H needs only suitably average the h-sampled data to guarantee that the guided rings are C^2. We found that piecewise polynomial C^1 guides with a straightforward averaging strategy are a viable option.
(d) If we consider a sequence of guide surfaces, it is sufficient to have the deviations from a single quadratic jet of the possibly different central jets of each sector vanish sufficiently fast.
(e) Observation 1 hints that the operator H can be replaced by mapping the jets directly to jets of the next refinement step [KMP06].
(f) By varying the common quadratic jet with each refinement step, we can create

a polar C^2 subdivision scheme of degree (6,4) that refines a control net. Since the rules are derived from guided subdivision, they involve the entire control net of the previous iteration.
(g) Both ρ and H can vary with m and even i.
(h) Rational guides and C^2 patchworks can be constructed by applying the approach in homogeneous space. Lemma 4 then implies that quadratic surfaces, for example spheres, can be reproduced.
(i) The guide principle can be applied to other box splines.
(j) We have used guided rings with good results to transition to a finite, low-degree piecewise polynomial cap for many-sided surface gaps.

Acknowledgement: This work was supported by NSF Grant CCF-0430891 and DMI-0400214.

References

[KMP06] K. Karčiauskas, A. Myles, and J. Peters. A C^2 polar jet subdivision. In A. Scheffer and K. Polthier, editors, *Proceedings of Symposium of Graphics Processing (SGP), June 26-28 2006, Cagliari, Italy*, 173–180. ACM Press, 2006.

[KP04] K. Karčiauskas and J. Peters. Polynomial C^2 spline surfaces guided by rational multisided patches. In T. Dokken and B. Jüttler, editors, *Algebraic Techniques in Geometric Design*. Springer, 2004.

[KP06a] K. Karčiauskas and J. Peters. On the curvature of guided subdivision surfaces. in preparation.

[KP06b] K. Karčiauskas and J. Peters. Surfaces with polar structure. *Computing*, pages xx+1–8, 2006. to appear.

[KPR04] K. Karčiauskas, J. Peters, and U. Reif. Shape characterization of subdivision surfaces – Case studies. *Computer Aided Geometric Design*, 21(6):601–614, july 2004.

[PR98] J. Peters and U. Reif. Analysis of generalized B-spline subdivision algorithms. *SIAM J of Numer. Anal.*, 35(2):728–748, April 1998.

[Pra97] H. Prautzsch. Freeform splines. *Comput. Aided Geom. Design*, 14(3):201–206, 1997.

[Pra98] H. Prautzsch. Smoothness of subdivision surfaces at extraordinary points *Adv. in Comp. Math.*, 9: 377-390, 1998.

[Rei95] U. Reif. A unified approach to subdivision algorithms near extraordinary vertices. *Comp Aided Geom Design*, 12:153–174, 1995.

[Rei96] U. Reif. A degree estimate for subdivision surfaces of higher regularity. *Proc. Amer. Math. Soc.*, 124(7):2167–2174, 1996.

[Rei98] U. Reif. TURBS—topologically unrestricted rational B-splines. *Constr. Approx.*, 14(1):57–77, 1998.

[Uml99] G. Umlauf. *Glatte Freiformflächen und optimierte Unterteilungsalgorithmen*. PhD thesis, 1999.

[WW02] Joe Warren and Henrik Weimer. *Subdivision Methods for Geometric Design*. Morgan Kaufmann Publishers, San Diego, CA, 2002.

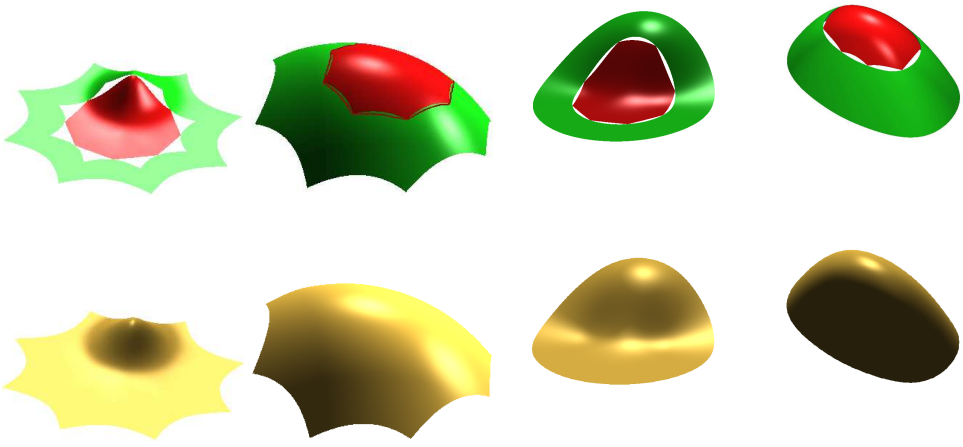

Figure 15: Partial gallery of test shapes. (*top*) Input rings (outer surface rings, *green*) and guides (inner surface pieces, *red*) ; (*bottom*) guided surfaces: from *left* to *right*: construction of type $\square$-sprocket (Catmull-Clark) $(\rho_C, h^{6,6})$, Δ-sprocket (Loop) (ρ_L, h^8), C^2 polar $(\rho_p, h^{6,5})$ and G^2 polar $(\rho_g, h^{5,5})$.